Journal of Materials Chemistry C

Quantum Chemical Studies of Transition Metal Single-Atom Catalysts: Catalytic Descriptors Exploration

Journal:	*Journal of Materials Chemistry C*
Manuscript ID	TC-ART-03-2024-001052.R2
Article Type:	Paper
Date Submitted by the Author:	08-May-2024

Complete List of Authors:	Li, Bo; Guizhou Education University, Guizhou Provincial Key Laboratory of Computational Nano-Material Science, Institute of Applied Physics Zheng, Mingyue; Shandong Police College, Department of Investigation Lin, Shichen; Kyushu University, Interdisciplinary Graduate School of Engineering Sciences Gu, Fenglong; South China Normal University, MOE Key Laboratory of Environmental Theoretical Chemistry and SCNU Environmental Research Institute, Guangdong Provincial Key Laboratory of Chemical Pollution and Environmental Safety & School of Environment Jiang, Jun; University of Science and Technology of China, Key Laboratory of Precision and Intelligent Chemistry, School of Chemistry and Materials Science Jia, Chuanyi; Guizhou Education University, Guizhou Provincial Key Laboratory of Computational Nano-Material Science, Institute of Applied Physics

Journal of Materials Chemistry C

Quantum Chemical Studies of Transition Metal Single-Atom Catalysts: Catalytic Descriptors Exploration

Received 00th January 20xx,
Accepted 00th January 20xx

DOI: 10.1039/x0xx00000x

Bo Li[a],‡ Mingyue Zheng[b],‡ Shichen Lin,[c] Feng Long Gu[d], Jun Jiang[e], and Chuanyi Jia[a,*]

Spin states of transition metal (TM) based catalysts play important roles in their catalytic performances. However, the lack of intrinsic structure-property relationship greatly limits the rational control of spin states. Herein, we present a systemic first-principles study of O_2 activation, CO oxidation, H_2O dissociation, and CO_2 dissociation on TM (Fe, Co, and Ni) single-atom catalysts (SACs) with different spin states. Calculation results indicate that the spin population can be changed by reactant adsorption in the catalytic processes. Through rational manipulation of TM type and spin, the activity of TM-SAC can be significantly improved. To shed light on the enhancement mechanism and explore some universal descriptors for TM-SACs, a series of structure-property relationships were systemically surveyed. It is found that the interactions between TM and O are very crucial for the binding stability/reactivity of the oxygen-containing reactants. Accordingly, the parameters that can reflect TM and O interactions, including TM-O bond length, key-species (O_2), spin moment, and charge transfer (charge on reactant), are all good descriptors for the catalytic performances of different models. More intriguingly, the novel spectral descriptors, such as the stretching vibrational frequency of TM-O/O-O/O-H, were found to have good linear relationship with the reactivity as well.

1. Introduction

Catalysts based on supported noble-metals exhibits excellent activities for many important chemical processes, including CO_2 reduction, CO oxidation, hydrogen evolution, and oxygen reduction reaction.[1-5] The scarcity and high cost of noble-metals, however, seriously hinder their large-scale practical applications. Searching for cost-effective yet efficient catalysts to substitute noble metals has therefore become a central task in catalysis chemistry and materials science.[6-10] Among others, transition metal (typically refers to Fe, Co, and Ni) single-atom catalysts (TM-SACs) have drawn increasing intense attention due to their high atom utilization and outstanding catalytic activity.[11-15]

It is widely recognized that the catalytic performance of TM-SAC is strongly related to spin state of the single metal center.[16-20] Thus, the rational control of spin states on TMs is extremely important for high catalytic performance. As yet, using traditional regulation methods, such as doping hetero-atoms, creating surface defects, changing TM's valence state, and importing external magnetic field,[20,21-25] the TM-SACs with different spin states have been extensively investigated. However, the strategies for the precise control of spin states are still limited and the underlying structure-property relationships between electronic/structural effects and catalytic property remain unclear.

Compared with commonly used metal/metal-oxide support, graphene-like material, especially N-doped graphene, has a simple two-dimensional structure but novel properties. In this regard, single transition metal catalysts anchored on N-doped graphene (TM-NC) have attracted a great deal of attention because of their remarkable catalytic performance and economic applicability.[26-30] On the other hand, exclusively dispersed active site with little interference from other metals provides a good entry to explore the influence of spin on activity. Based on Fe-SACs, research by Li et al. has shown that the spin-crossover effect on N-FeN_4C_{10} moiety plays important roles in the catalytic activity, which makes it become more favorable for oxygen reduction than other models.[31] In addition, Rao et al. also observed significant electronic structure evolution of single Co atom on NC, in which the local magnetic moment of Co active site varies during its whole catalytic process.[32] In another intriguing work, Liu et al. indicated that the Fe(III)N_5 structured active center with proper spin state owns at least one order of magnitude higher oxidation activity than Fe(III)N_6 centers.[33] Likewise, our recent theoretical study showed that the electronic spin moment of Fe-C_2N has close relationship with the catalytic performance as well.[34]

[a] *Guizhou Provincial Key Laboratory of Computational Nano-Material Science, Institute of Applied Physics, Guizhou Education University, Guiyang, Guizhou 550018, China. E-mail: cyjia@gznc.edu.cn*
[b] *Department of Investigation, Shandong Police College, Jinan, Shandong 250200, China*
[c] *Interdisciplinary Graduate School of Engineering Sciences, Kyushu University, 6-1 Kasuga-Park, Fukuoka 816-8580, Japan*
[d] *MOE Key Laboratory of Environmental Theoretical Chemistry and SCNU Environmental Research Institute, Guangdong Provincial Key Laboratory of Chemical Pollution and Environmental Safety & School of Environment, South China Normal University, Guangzhou 510006, China*
[e] *Key Laboratory of Precision and Intelligent Chemistry, School of Chemistry and Materials Science, University of Science and Technology of China, Hefei, Anhui 230026, China*

†Electronic Supplementary Information (ESI) available: See DOI: 10.1039/x0xx00000x

‡The first two authors contributed equally to this work.

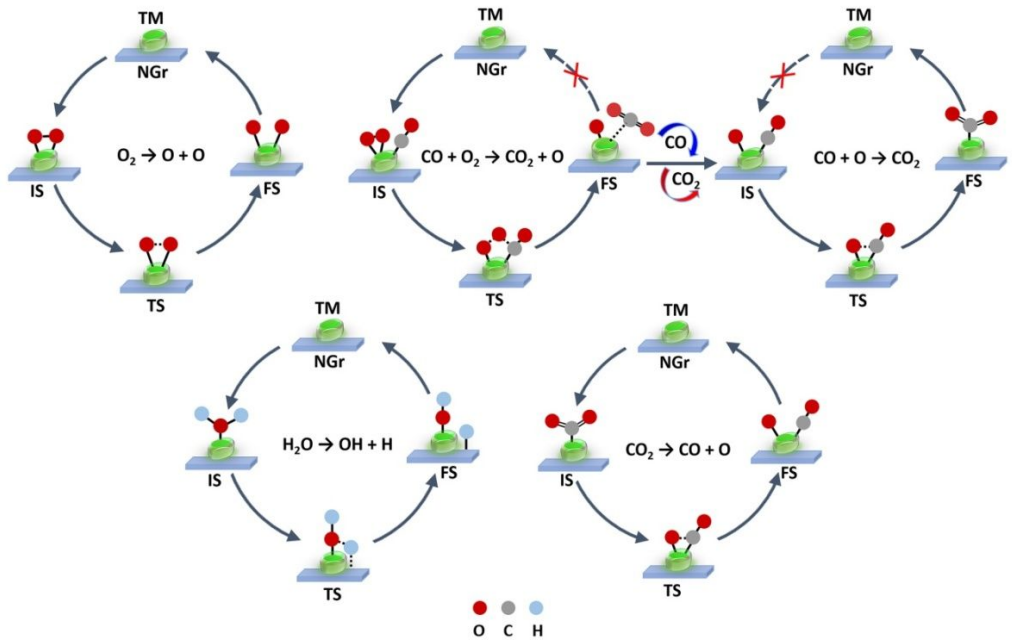

Figure 1. Schematic diagrams of O_2 activation, CO oxidation, H_2O dissociation, and CO_2 dissociation.

Although TM-SACs with different spin states have been widely studied, the majority of researches are mainly focused on a certain catalyst and reaction. Comprehensive investigations and comparisons for different catalysts and reactions are still lacked until recently. Here, in order to systemically elucidate the enhancement mechanisms of TM-SACs and explore some catalytic descriptors for the rational design of related catalysts, a detailed research for NC supported Fe, Co, and Ni (including TM(II) and TM(III)) single atoms with different spin states are performed. The reliability and universality of the proposed influence mechanisms are verified by four commonly used reactions,[35-39] including O_2 activation, CO oxidation, H_2O dissociation, and CO_2 dissociation (Figure 1).

2. Methods

All quantum chemistry calculations in this work were carried out at the density functional theory (DFT) level of M06-L functional via Gaussian16 package.[40,41] The reliability of this method for TM system calculations has been verified by various theoretical and experiment researches.[23,34,42-45] The unrestricted formalism of M06-L functional was adopted to calculate the high spin states (S > 0). The def2-SVP basis set was selected for C, H, N, and O atoms, and the Stuttgart/Dresden (SDD) basis set was utilized to describe Fe, Co, and Ni atoms, both of which are commonly used basis sets for corresponding systems.[43-47] The Grimme's DFT-D3 scheme was used to deal with the long-range van der Waals (vdW) interactions.[48] The vibrational frequency calculations were added for: (1) confirming geometrical structures as minima (zero imaginary frequency); (2) verifying the accuracy of the geometries for transition state (TS, only one imaginary frequency); (3) providing free energies at 298.15 K. The intrinsic reaction coordinates (IRC) were also performed to verify that the configurations of TS connect two relevant minima.[49,50] The spin density and electronic spin moments (μ_B) were obtained by open-access Multiwfn package.[51] The rectangular graphene monolayer with graphitic-N was used to reflect the NC support, whose reliability have been repeatedly verified by many theoretical/experimental studies.[52-55]

3. Results and discussion

3.1. Catalytic mechanisms of different reactions on TM-SACs

As we know, the N_3-coordinated and N_4-coordinated TMs (TM-N_3 and TM-N_4) are both commonly used models for theoretical and experimental studies.[18,20,26,37,38,56,57] To select a more reasonable SAC model for further studies, detailed comparisons between Fe-N_3 and Fe-N_4 with same spin state (S = 1) are performed. The calculation results in Figure S1 indicate that the binding stabilities of different reactants on Fe-N_4, including O_2, CO+O_2, CO+O, H_2O, and CO_2, are all much lower than that on Fe-N_3 (Table 1). This conclusion fits well with our previous work on TM_2-NC.[58] Moreover, the CO+O_2 and H_2O with positive adsorption Gibbs free energies even cannot spontaneously adsorbed on Fe-N_4. As a result, the TM-N_3 geometry with more favorable binding stabilities of oxygen-containing reactants is selected for the following activity investigations.

As a start, the stabilities of the TM-SACs are first discussed. From Table S1, one can see that the most stable spin state for different TMs are Fe(III)(S = 1/2) (-160.50 kcal/mol), Co(II)(S = 1/2) (-190.89 kcal/mol), and Ni(II)(S = 1/2) (-227.25 kcal/mol), respectively. Due to the much higher binding energies of TMs (≥ -80.22 kcal/mol) compared to reaction barriers (≤ 42.11 kcal/mol, Table 1), the TMs all can stably exist under reaction conditions. The identified stable geometries of TM-SACs with low spin state (S = 0) are illustrated in Figure S2. The electronic spin moments under different spin states are in the range of 0.00-3.52 μ_B for Fe, 2.00-2.66 μ_B for Co, and 1.62-1.69 μ_B for Ni, respectively (Table S2). From Figure S3, one can see that the spin is dispersed on Fe and surface C atoms in clean Fe-NC surface. However, when reactant adsorption occurs, e.g. O_2, the spin becomes concentrated near the Fe active center (Figure 2). For Co and Ni, the spin is concentrated near the active center as well, especially after O_2 adsorption (Figures S4-S7). This is because the most

Table 1. Adsorption Gibbs free energies (ΔG_{ads}, kcal/mol) and corresponding energy barriers (EB, kcal/mol) of O_2 activation, CO+O_2, CO+O, H_2O dissociation, and CO_2 dissociation.

	O_2		CO+O_2		CO+O		H_2O		CO_2	
	ΔG_{ads}	EB	ΔG_{ads}	EB	ΔG_{ads}	EB	ΔG_{ads}	EB	ΔG_{ads}	EB
Fe(II)(S=0)	-40.06	29.77	-60.73	31.02	-49.91	4.42	-13.88	33.01	-2.37	30.60
Fe(III)(S=1/2)	-44.58	—	-64.44	27.48	-60.13	5.69	-18.73	35.37	-18.85	38.12
Fe(II)(S=1)	-75.18	18.33	-79.87	26.25	-86.12	3.72	-29.39	31.12	-35.06	26.38
Fe(III)(S=3/2)	-62.63	21.64	-66.14	27.63	-71.54	4.10	-35.90	16.63	-21.02	27.29
Fe(II)(S=2)	-49.59	—	-45.28	13.46	-59.64	3.62	-16.28	24.06	-9.58	27.28
Fe(III)(S=5/2)	-45.66	17.02	-40.63	15.33	-54.29	4.13	-18.96	16.95	-6.63	30.19
Co(III)(S=0)	-47.34	—	-64.53	19.11	—	—	-17.58	32.87	-6.15	—
Co(II)(S=1/2)	-41.85	26.03	-50.54	16.48	-44.25	2.28	-10.89	27.04	-7.37	39.11
Co(III)(S=1)	-34.09	27.89	-41.84	17.15	-35.79	2.83	-18.44	39.88	-1.36	42.11
Co(II)(S=3/2)	-39.60	25.89	-45.35	26.81	-41.93	2.13	-17.59	28.45	-5.36	39.28
Co(III)(S=2)	-34.02	27.61	-39.59	29.07	-35.67	2.93	-19.23	41.83	-1.11	42.08
Co(II)(S=5/2)	-47.70	—	-54.83	17.49	-54.66	8.06	-14.94	25.17	-0.58	27.70
Ni(II)(S=0)	—	—	—	—	—	—	—	—	—	—
Ni(III)(S=1/2)	-28.93	34.30	-35.39	29.58	—	—	-16.13	27.68	0.10	—
Ni(II)(S=1)	-32.11	31.29	-37.84	16.90	—	—	-14.19	28.30	-3.05	—
Ni(III)(S=3/2)	-29.24	35.14	-35.73	30.01	-23.05	—	-17.43	20.99	0.12	—
Ni(II)(S=2)	-45.44	—	-51.23	14.98	-38.64	1.63	-13.43	24.46	-0.22	36.93
Ni(III)(S=5/2)	-42.16	35.35	-48.52	—	-35.81	4.27	-15.12	18.22	6.62	35.56

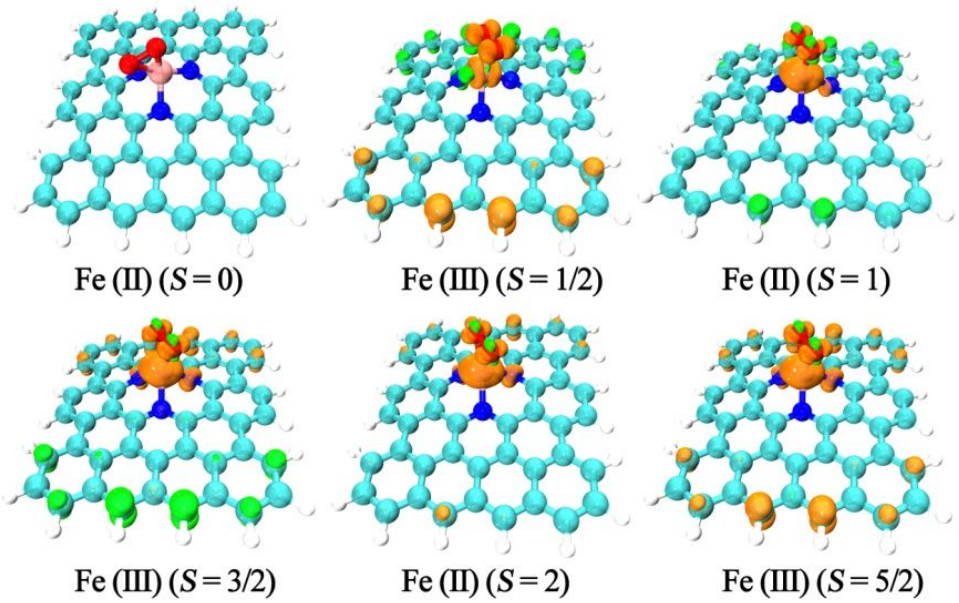

Figure 2. Structures and spin densities (isovalue is 0.009) of O_2 adsorption on NC supported Fe(II) and Fe(III) SACs with different spin states. Fe atoms are in pink, C in cyan, H in white, and N in deep blue.

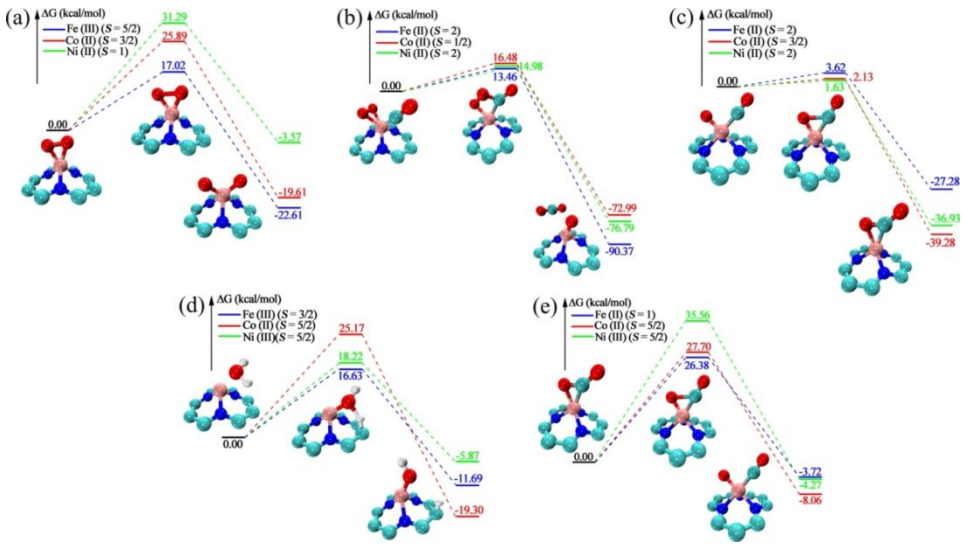

Figure 3. Calculated potential energy profiles of the O_2 activation (a), CO oxidation (b, c), H_2O dissociation (d), and CO_2 dissociation (e) on NC supported Fe, Co, and Ni SACs. For each metal, the optimal spin state with lowest energy barrier is listed. The optimized geometry of Fe-SAC for each reaction is selected as an example. O atoms are in red, others are the same as Figure 2.

prominent charge transfer occurs at the interfacial site between catalyst and reactant. This phenomenon can easier induce electron aggregation, leading to the localization of electrons and spin density near the metal center.[34] Then, the localized electrons and spin density can further promote the charge transfer between TM-SAC and reactant, which plays important roles in the change of TM spin moment and catalytic performance during the following reaction processes.[59]

For O_2 adsorption, the binding free energies (ΔG_{ads}) on Fe-NC under different spin states are ranging from -75.18 to -40.06 kcal/mol (Table 1). Among Fe(II) models, the ground state of O_2 adsorption is the spin state of S = 1, whose binding energy is lower than that of S = 2 and S = 0 by 25.59 and 35.12 kcal/mol, respectively. Similarly, the Fe(III) with S = 3/2 has higher O_2 binding stability than other two spin states (S = 1/2 and 5/2) as well. The O_2 capture capacity on Fe follows the order of: Fe(II)(S = 1) > Fe(III)(S = 3/2) > Fe(II)(S = 2) > Fe(III)(S = 5/2) > Fe(III)(S = 1/2) > Fe(II)(S = 0). Concisely, comparing all the three metals with optimal binding stabilities, the priority order of O_2 adsorption is Fe(II)(S = 1) > Co(II)(S = 5/2) > Ni(II)(S = 2). Then, for O_2 dissociation, no stable products on Fe(II)(S = 2) and Fe(III)(S = 1/2) were obtained. The energy barriers of the residual four Fe-NC models show that Fe(III)(S = 5/2) with lowest energy barrier of 17.02 kcal/mol is more active than others. This model even performances better than Fe-SACs on C_2N.[34] Based on overall O_2 dissociation barriers comparison, the most active spin states for each metal are Fe(III)(S = 5/2), Co(II)(S = 3/2), and Ni(II)(S = 1), respectively. The potential energy profiles in Figure 3a clearly show that O_2 activation on Fe(III)(S = 5/2) is more suitable than that on Co(II)(S = 3/2) and Ni(II)(S = 1), due to its much lower energy barrier.

Following O_2 activation, a more complex research for CO oxidation is performed. As it can be seen from Figure 1, CO oxidation occurs on TM-SACs via a two-step mechanism: (i) CO + O_2 → CO_2 + O, and (ii) CO + O → CO_2. According to the binding energies in Table 1, the ground states of co-adsorbed CO and O_2 on different TMs are Fe(II)(S = 1) (-79.87 kcal/mol), Co(III)(S = 0) (-64.53 kcal/mol), and Ni(II)(S = 2) (-51.23 kcal/mol), respectively. Similar to O_2, the order of co-adsorption stability is Fe > Co > Ni. Then, the co-adsorbed CO and O_2 react to form a CO_2 and a residual *O on TM (Figure 3b). The reaction barriers of the best states on different metals are 13.46 kcal/mol on Fe(II)(S = 2), 16.48 kcal/mol on Co(II)(S = 1/2), and 14.98 kcal/mol on Ni(II)(S = 2), respectively. With the completion of CO+O_2 reaction, the residual *O on TM directly reacts with an additional CO molecule, via a much lower energy barrier (EB ≤ 8.06 kcal/mol, Figure 3c and Table 1). It is largely because of the fact that the unsaturated *O is a very active intermediate, which can easily interact with other reactants. Obviously, the CO+O_2 reaction with much higher energy barrier is the rate-determining step for CO oxidation on these TM-NC models. From the CO+O_2 catalytic processes in Figure 3b, one can see that the overall reactivity of the TMs follows the order of: Fe(II)(S = 2) > Ni(II)(S = 2) > Co(II)(S = 1/2).

Specifically, the binding stabilities of H_2O with ΔG_{ads} ranging from -35.90 to -10.89 kcal/mol are much lower than that of O_2/CO+O_2/CO+O on corresponding TM models (Table 1). The priority order of H_2O adsorption on different metals is Fe(III)(S = 3/2) (-35.90 kcal/mol) > Co(III)(S = 2) (-19.23 kcal/mol) > Ni(III)(S = 3/2) (-17.43 kcal/mol). The calculated potential energy profiles in Figure 3d show that the dissociated H atom is more inclined to bind on the adjacent C atom, with OH binding on the metal site. The reaction barriers of the most active states on different metals follow the order of Fe(III)(S = 3/2) (16.63 kcal/mol) < Ni(III)(S = 5/2) (18.22 kcal/mol) < Co(II)(S = 5/2) (25.17 kcal/mol). Consequently, Fe(III)(S = 3/2) with larger reactant binding stability and lower reaction barrier should be the best model for H_2O dissociation.

As an important methodology for CO_2 emission abatement, thermocatalytic CO_2 dissociation has drawn increasingly intense attention in the past decades.[60-62] Note that CO_2 is an inert molecule, which is difficult to catch in thermocatalytic environment. Thus, the capture capacity of CO_2 is quite essential for further dissociation reaction. The negative values of ΔG_{ads} on

Fe-NC under different spin states (Table 1) indicate that CO_2 adsorptions on Fe models are all exothermic and spontaneous processes. Moreover, the Fe(II)(S = 1) with much lower ΔG_{ads} (-35.06 kcal/mol) should be the ground state of CO_2 adsorption. Then, comparing all the TM models in Table 1, the tendency of binding stability on different metals follows the order of: Fe(II)(S = 1) (-35.06 kcal/mol) > Co(II)(S = 1/2) (-7.37 kcal/mol) > Ni(II)(S = 1) (-3.05 kcal/mol). From Figure 3e, one can see that the dissociation barriers of the best states on different metals are 26.38 kcal/mol on Fe(II)(S = 1), 27.70 kcal/mol on Co(II)(S = 5/2), and 35.56 kcal/mol on Ni(III)(S = 5/2), respectively. The lower reaction barrier in combination with its much higher capture capacity of CO_2 suggest that the Fe(II)(S = 1) should be the most favorable model for CO_2 dissociation.

Finally, from the detailed comparisons in Figure 4, the most favorable catalysts for ΔG_{ads}/EB of different reactions are identified as follows: Fe(II)(S = 1)/Fe(III)(S = 5/2) for O_2 activation; Fe(II)(S = 1)/Fe(II)(S = 2) for CO oxidation; Fe(III)(S = 3/2)/Fe(III)(S = 3/2) for H_2O dissociation; and Fe(II)(S = 1)/Fe(II)(S = 1) for CO_2 dissociation. Clearly, the Fe-containing models generally performance better than other two TMs. This phenomenon is benefiting from the stronger oxytropism of Fe atom (Table 1).[58,63] Larger interactions between Fe active center and oxygen-containing reactants can promote the pre-activation of the O-O/C-O/O-H bonds, resulting in higher binding stability and reactivity. Similar conclusion was obtained for TM_2-NC in our previous work.[58] Thus, if we want to synthesize efficient catalysts for oxygen-containing reactants, the Fe-containing materials should be considered first.

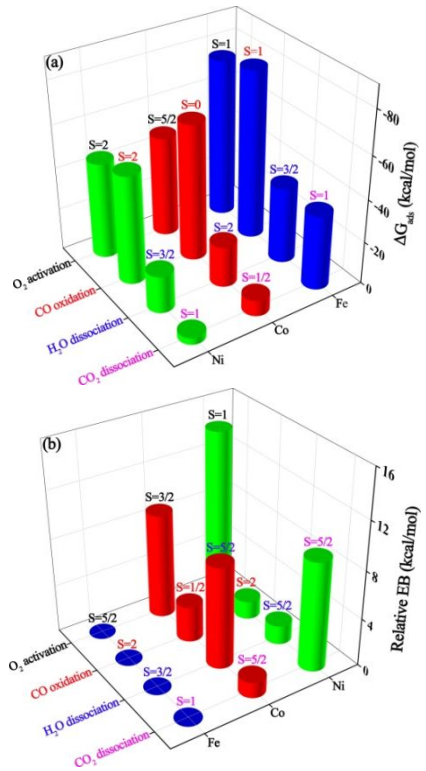

Figure 4. Comparisons of reactant binding energies (a) and relative energy barriers (b, EBs of Fe are set to zero) of optimal Fe, Co, and Ni SACs for different reactions.

It is important to point out that the desorption of molecular product in the reaction is an important step for the recycle of active site. As a result, the desorption processes of the steps containing molecular products (such as the CO_2 molecule in CO + O_2 → CO_2 + O and CO + O → CO_2, and the CO molecule in CO_2 → CO + O) are further discussed. The desorption of CO_2 in CO + O_2 step reveals that the CO_2 products all have much lower desorption energies than their corresponding reaction barriers (Table S3). Thus, the desorption process, with released free CO_2 molecule and residual *O-TM, can easily occur on TM-SACs. For the following CO + O step, only the desorption of CO_2 on Fe(II)(S = 1) (35.06 kcal/mol) has higher energy than the reaction barriers of CO + O_2 (26.25 kcal/mol) and CO + O (3.72 kcal/mol). Thus, the rate determining step for CO oxidation changes to the final CO_2 desorption on Fe(II)(S = 1). From the detailed comparison for the reaction and desorption barriers in Tables 1 and S3, the optimal model for CO oxidation should be the Fe(II)(S = 2). Then, for the desorption process of CO in CO_2 dissociation (with released free CO molecule and residual *O-TM), most of the desorption energies are higher than the reaction barriers of CO_2 → CO + O. The energy barrier of the rate determining step in Table S3 shows that the Co(II)(S = 5/2) is the optimal model for dissociation of CO_2 to produce CO. However, if we want to use adsorbed CO for further reactions (such as hydrogenation reactions), the desorption of CO is not necessary for subsequent steps, and Fe(II)(S = 1) with lower CO_2 → CO + O reaction barrier will have better performances than other models (Table 1). Similarly, for the atomic products, such as *O, *H, and *OH, because they are all intermediates for further reactions, the desorption of them has little influence on the recycle of active sites.

The above analysis reveals that via rational control of TM type and spin state, the catalytic performance of TM-SAC can be obviously improved. However, there is no discernible rule between the activity and spin. As we know, catalytic descriptors provide a facile way for the revelation of the intrinsic catalytic mechanism and rational design of high-efficient catalysts. Thus, to explore some universal descriptors for these TM-SAC models, multifarious structure-property relationships are further analyzed.

3.2. Quantitative structure-property relationships analysis of TM-SACs

3.2.1. Catalytic roles of traditional descriptors. As a start, the most commonly studied correlation between reactant binding stability and reactivity is first illustrated.[58,64,65] As expected, we obtained a linear relationship between all of the ΔG_{ads} and corresponding EB in O_2 activation, CO oxidation, H_2O dissociation, and CO_2 dissociation, with correlation coefficient r = 0.58 (Figure 5a). The determined trend that EB decrease with the increase of reactants binding stability further supports the reliability to adopt ΔG_{ads} as a descriptor for catalytic activities. However, the low correlation coefficient for this linear relationship indicates that the binding stability of corresponding reactant is a weakly correlated descriptor for NC supported SACs and can only be used to roughly estimate the catalytic performance.

It is known that the strength of TM-O bonds usually plays important roles in the binding stability/reactivity of adsorbates that contain O atoms. Accordingly, the bond length of TM-O (L(TM-O)) which can reflect the interaction strength between TM and O atoms offers a good parameter to estimate the binding energy/energy barrier. In Figure 5b and 5c, we list the linear relationships between L(TM-O) and ΔG_{ads}/EB. Specifically, the O_2 and CO+O_2 reactants have two TM-O bonds. For easy comparison, the average bond lengths are used for these models. The correlation coefficients for these two linear relationships are

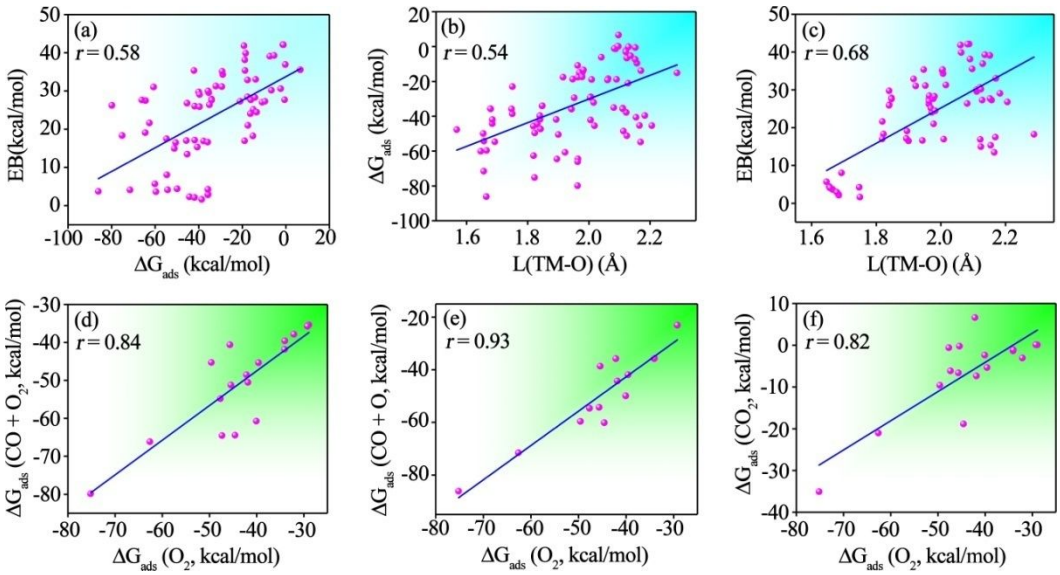

Figure 5. Correlation between the binding stability (ΔG_{ads}) and energy barrier (EB) (a); correlations between the TM-O bond length (L(TM-O), detailed data is shown in Table S4) and ΔG_{ads}/EB (b, c); correlations between the ΔG_{ads} of O_2 and ΔG_{ads} of CO+O_2 (d), CO+O (e), and CO_2 (f). Colored backgrounds indicate the change trends of the linear relationships.

0.54 and 0.68, respectively. Their similar change trend suggests that shorter TM-O bond length is more favorable for reactant binding stability and reactivity. In view of the low correlation coefficient (r = 0.54), the L(TM-O) should be a weakly correlated descriptor for binding stability as well. However, for the reactivity, the L(TM-O) (r = 0.68) has much better performance than ΔG_{ads} (r = 0.58).

Following L(TM-O), the O_2 binding stability that can also reflect the interaction strength between TM and O atoms is further discussed. In Figures 5d-5f and S8, we show the correlations between the binding energies of O_2 and CO+O_2/CO+O/CO_2/H_2O. These four good linear relationships confirm the feasibility and universality of using the $\Delta G_{ads}(O_2)$ as a key-species descriptor for oxygen-containing adsorbates, especially for CO+O_2 (r = 0.84), CO+O (r = 0.93), and CO_2 (r = 0.82). Thus, compared to L(TM-O), the $\Delta G_{ads}(O_2)$ is a more precise descriptor for the binding stability of oxygen-containing adsorbates. However, for reactivity, the O_2 dissociation barrier (EB(O_2)) as a key-species descriptor for CO+O_2 (r = 0.34), CO+O (r = -0.04), H_2O dissociation (r = 0.07), and CO_2 dissociation (r = 0.54) has a poor performance (Figure S9).

3.2.2. Catalytic roles of electronic descriptors. To explore more intrinsic relationships between catalytic performance and spin, various spin-correlated descriptors are further analyzed. As mentioned above, the spin on clean TM-SAC is dispersed on TM and surface C atoms (Figure S3). After O_2 adsorption, the dispersed spin becomes mainly located near the active center (Figure 2). Clearly, the change of spin induced by O_2 adsorption takes place primarily near the TM atom. As a result, the change of spin moments ($\Delta\mu_B$) of TM under different spin states should be closely related to the interactions between TM-SAC and O_2. Intriguingly, we found a good linear relationship between $\Delta\mu_B$(TM-O_2) and $\Delta G_{ads}(O_2)$ (r = -0.76, Figure 6a). The change trend implies that more positive spin moment variations before and after O_2 adsorption may reflect stronger binding stabilities. Similarly, the cases for other two single-molecule reactants (H_2O/CO_2) have good linear relationships as well (r = -0.87 and -0.85, respectively, Figure 6b and 6c). However, for multi-molecule reactants (CO+O_2/CO+O), due to their more complex interactions between TM and adsorbates, the $\Delta\mu_B$ parameter has poor performance (r = -0.19 and -0.38, respectively, Figure S10a and S10b). Thus, the change of spin moments of TM for corresponding reactants ($\Delta\mu_B$(TM-Reactant)) as a binding stability descriptor has limitations in wide applications.

Note that the O_2 binding stability as a key-species descriptor can well reflect the binding stability of other oxygen-containing reactants. Inspired by this design concept, we applied a novel $\Delta\mu_B$(TM-O_2) parameter. Not surprisingly, the $\Delta\mu_B$(TM-O_2), owing to their good linear relationships with the ΔG_{ads} of CO+O_2 (r = -0.82), CO+O (r = -0.74), CO_2 (r = -0.78), and H_2O (r = -0.61), demonstrates great potential as an indicator for the binding stabilities of other oxygen-containing reactants (Figures 6d-6f and S10c). Then, for reactivity, however, no reliable and universal rule is obtained for $\Delta\mu_B$(TM-O_2)/$\Delta\mu_B$(TM-Reactant), as shown in Figure S11 and S12. Therefore, the $\Delta\mu_B$(TM) descriptors can only be selectively used to estimate the binding stabilities of reactants.

Besides spin moment, the charge transfer (Δq, equal to the charge on reactant) also has great influence on the interactions between TM-SACs and reactants. To shed light on the catalytic role of charge transfer, the correlations between Δq and ΔG_{ads}/EB are further studied, as shown in Figure 7a and 7d. The change trend of the linear relationship indicates that larger charge transfer from SAC to reactant is more favorable for binding stability and reactivity. However, the low correlation coefficients (r = 0.56 and 0.53, respectively) suggest that the Δq (charge transfer of the corresponding reactant) descriptor is a weakly correlated descriptor for ΔG_{ads}/EB. Following the design concept of $\Delta\mu_B$(TM-O_2), the $\Delta q(O_2)$ as a key-species descriptor is imported. The good linear relationships in Figure 7b and 7e show that the $\Delta q(O_2)$ can well reflect its own binding stability and energy barrier (r = 0.74 and 0.85, respectively). Then, as a key-species descriptor, $\Delta q(O_2)$ can be used to estimate the binding stability of other oxygen-containing reactants as well (strongly correlated for CO_2, CO+O_2, and CO+O; weakly correlated for H_2O), as shown in Figures 7c and S13. However, for reactivity, only CO_2 has good linear relationships (r = 0.63, Figures 7f and S13). Thus, the $\Delta q(O_2)$ is not a universal descriptor for catalytic activity, which can only be selectively used for O_2 and CO_2.

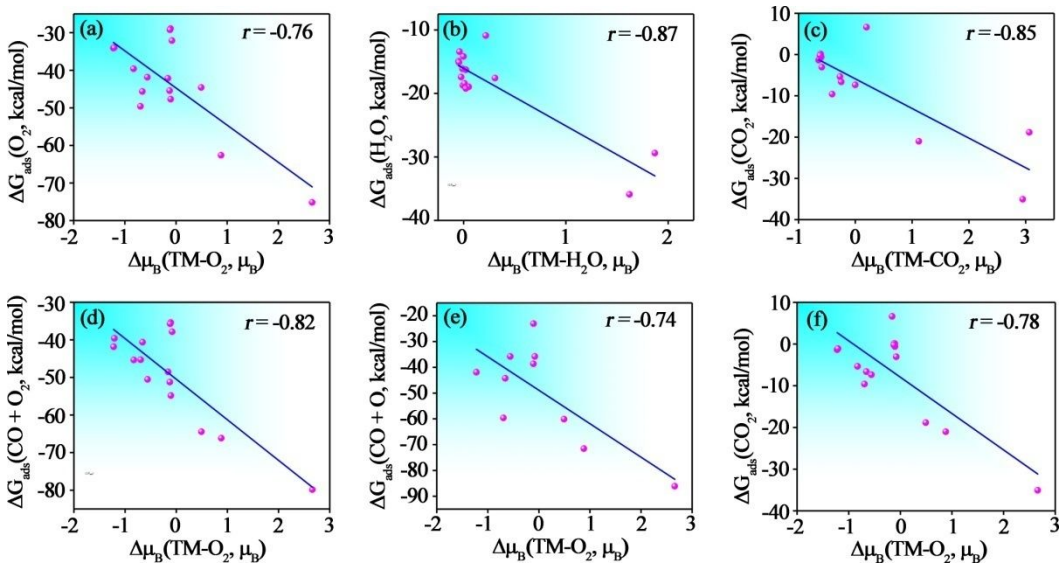

Figure 6. Correlations between the variation of electronic spin moment ($\Delta\mu_B$) of TM (before and after reactants adsorption) and ΔG_{ads} of O_2 (a), H_2O (b), and CO_2 (c). Correlations between the $\Delta\mu_B$ of TM (before and after O_2 adsorption) and ΔG_{ads} of CO+O_2 (d), CO+O (e), and CO_2 (f). Detailed data is shown in Table S2. Colored backgrounds indicate the change trends of the linear relationships.

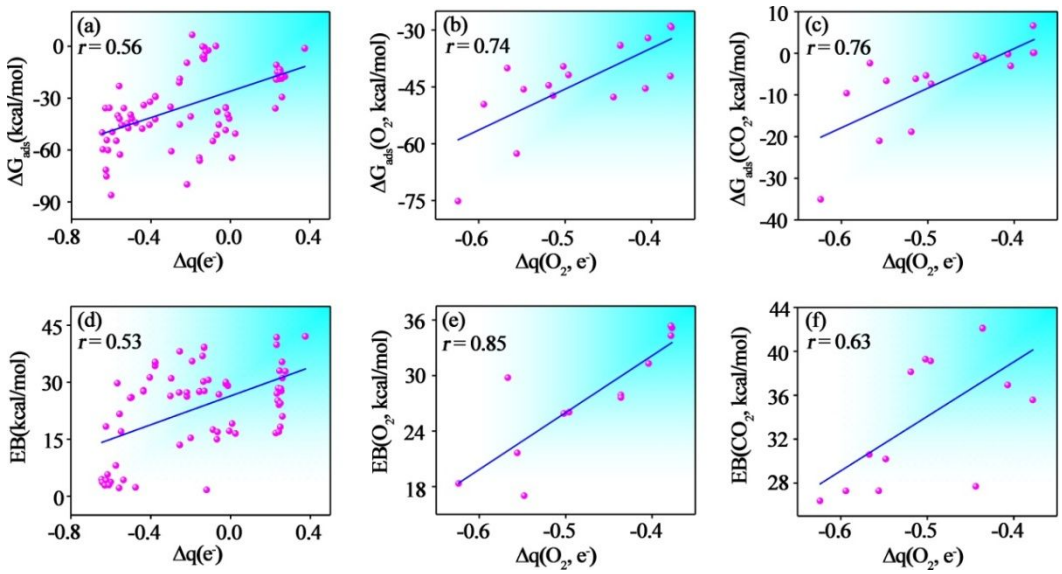

Figure 7. Correlations between the charge on reactant (Δq, after adsorption) and ΔG_{ads}/EB (a, d); correlations between the charge on O_2 ($\Delta q(O_2)$, after adsorption) and ΔG_{ads}/EB of O_2 (b, e); correlations between $\Delta q(O_2)$ and ΔG_{ads}/EB of CO_2 (c, f). Detailed data is shown in Table S5. Colored backgrounds indicate the change trends of the linear relationships.

To explore more useable descriptors for oxygen-containing reactants, the novel $\Delta\mu_B$(TM-O) and Δq(O), corresponding parameters after single O atom adsorption, are calculated and analyzed. From Figure S14, we note that the $\Delta\mu_B$(TM-O) as a more concise descriptor than $\Delta\mu_B$(TM-O_2) can be applied to estimate the binding stabilities of different reactants as well: strongly correlated for O_2 (r = -0.60), CO+O_2 (r = -0.82), CO+O (r = -0.64), and CO_2 (r = -0.74); weakly correlated for H_2O (r = -0.47). For reactivity, however, no reliable relationship is obtained (Figure S15). Then, for Δq(O), only the binding stability and reactivity of O_2, with r = 0.52/0.52, have weak relationships ($r \leq 0.42$ for others, Figures S16 and S17).

3.2.3. Catalytic roles of spectral descriptors. From the above analysis, we note that the TM and O interactions play key roles in the catalytic performances of oxygen-containing reactants on TM-SACs. As a rule, larger TM and O interactions usually results in a stronger/shorter TM-O bond, and enhances the stretching vibration frequency. The determined trend that L(TM-O) decreases with increasing TM-O stretching vibrational frequency (ν(TM-O), r = -0.79, Figure 8), further confirms the reliability of this conclusion. Consequently, similar to L(TM-O), the ν(TM-O) can reflect the binding stability/reactivity of oxygen-containing reactants as well. In Figure 9a and 9e, we show the linear relationship between ν(TM-O) and ΔG_{ads}/EB. The low correlation coefficient for ΔG_{ads} (r = -0.44) indicates that ν(TM-O) is a weakly correlated descriptor for binding stability. However, for reactivity, the ν(TM-O) has much better performance (r = -0.73).

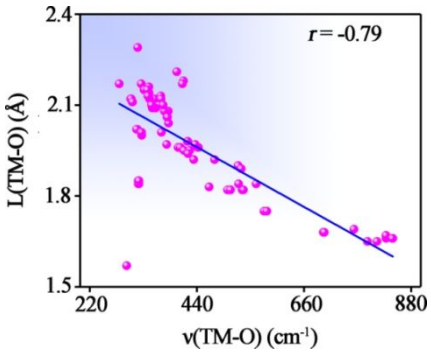

Figure 8. Correlation between the stretching vibrational frequency of TM-O (ν(TM-O)) and L(TM-O). Detailed data is shown in Tables S4 and S6. Colored background indicates the change trend of the linear relationship.

It is widely recognized that the O-O stretching vibration is the key vibrational characteristic of O_2.[58] Accordingly, to screen out more spectral descriptors for the rational design of TM-SACs, we broaden our research to cover the intrinsic spectroscopic properties of the reactants. Different from TM-O, larger adsorption strength can pre-activate O_2 more efficiently, leading to a weaker O-O bond and lower stretching vibration frequency. The trend that ΔG_{ads}/EB of O_2 increases with decreasing ν(O-O) fits well with this conclusion (Figure 9b and 9f). As expected, the ν(O-O) which represents the vibrational characteristic of the breaking bond in O_2 dissociation is more favorable for reactivity (r = 0.82) than binding stability (r = 0.58).

For other two dissociation processes of H_2O (r = 0.26) and CO_2 (r = 0.66), only ν(C-O) in CO_2 has useable correlation with corresponding binding stability (Figure 9c and 9d). Thus, the stretching vibration frequency of the breaking bond in reactants as a binding stability descriptor has limitations in universal applications. Then, for reactivity, the same direction of the correlation trend lines slope for ν(O-O), ν(O-H), and ν(C-O) further confirms that the pre-activation of the breaking bond in dissociated reactants is crucial for reactivity, as shown in Figure 9f-9h. In addition, the lower correlation coefficients for the linear relationships between ν(O-H)/ν(C-O) and corresponding EB (r = 0.68 and 0.46, respectively) suggest that more atoms in molecular is unfavorable for the accuracy of such descriptors. It is largely because of the fact that more atoms in molecular results in more complex interactions between different bonds in reactants. These additional interactions can significantly influence the stretching vibration frequency of the breaking bond, and further lower the descriptor's accuracy. In consequence, the adsorbed O_2 that has simple stretching vibration of breaking bond can reflect the dissociation activity much better than that for H_2O/CO_2. These spectral descriptors provide new strategies for experimentalists to estimate the activity of corresponding TM-SACs. Unfortunately, for $CO+O_2$ and CO+O reactions, whose key step is the generation of C-O bond, no new useable spectral descriptor is found for binding stability/reactivity, besides ν(TM-O).

4. Conclusion

In this work, various catalytic processes on a series of TM-SACs with different spin states are investigated using DFT calculations. The change of spin state on TM was found to be closely related to the catalytic performance. From overall catalytic processes comparison, we note that the Fe-containing models with optimal spin states are generally more active than other two TMs for all of the four reactions. To elucidate the intrinsic enhancement mechanism and explore some useful descriptors for the rational design of TM-SACs, lots of structure-property relationships were further surveyed. The results show that the TM and O interactions are very crucial for the reactant binding stability/reactivity. Hence, the parameters that have close relationship with TM and O interactions, including TM-O bond length, key-species (O_2), spin moment, and charge transfer, can act as good descriptors for the catalytic performances of TM-SACs. In addition, the stretching vibrational frequency of TM-O/O-O/O-H was found to have good linear relationship with the reactivity as well. It is our hope that the proposed electronic/structural effect can provide important insight into the influence mechanism of spin, thus enhancing our ability in designing new TM-SACs for practical applications.

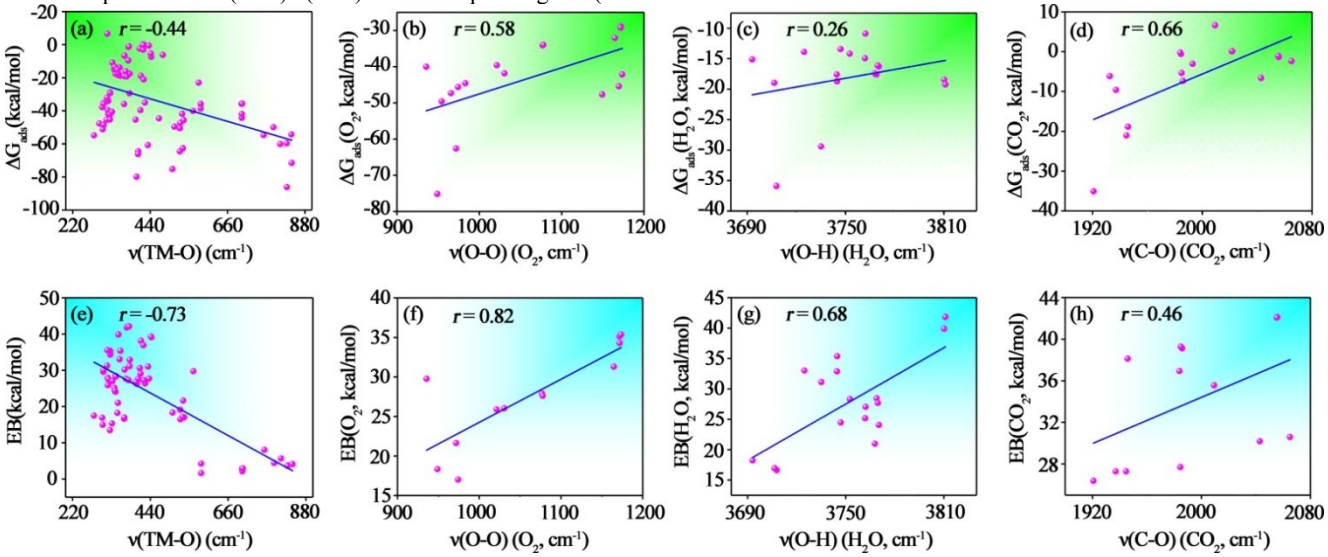

Figure 9. Correlations between the stretching vibrational frequency of TM-O (ν(TM-O)) and ΔG_{ads}/EB (a, e); correlations between the stretching vibrational frequency of O-O (ν(O-O)) and ΔG_{ads}/EB of O_2 (b, f); correlations between the stretching vibrational frequency of O-H (ν(O-H)) and ΔG_{ads}/EB of H_2O (c, g); correlations between the stretching vibrational frequency of C-O (ν(C-O)) and ΔG_{ads}/EB of CO_2 (d, h). Detailed data is shown in Table S6. Colored backgrounds indicate the change trends of the linear relationships.

CRediT authorship contribution statement

Bo Li: Data curation, Formal analysis, Funding acquisition, Investigation, Methodology, Project administration, Writing-original draft. **Mingyue Zheng:** Data curation, Formal analysis, Investigation, Methodology, Writing-original draft. **Shichen Lin:** Data curation, Formal analysis, Funding acquisition, Investigation, Project administration. **Feng Long Gu:** Funding acquisition, Project administration, Resources, Writing-review & editing, Supervision. **Jun Jiang:** Funding acquisition, Project administration, Resources, Writing-review & editing, Supervision. **Chuanyi Jia:** Conceptualization, Formal analysis, Funding acquisition, Investigation, Methodology, Project administration, Resources, Writing-original draft, Writing-review & editing.

Conflicts of interest

There are no conflicts to declare.

Acknowledgements

This work was financially supported by the Hefei Comprehensive National Science Center, the National Science Foundation of China (NSFC 22163002, 22203019), the Guizhou Provincial Science and Technology Projects (QKHJC-ZK[2021]YB047), the Scientific Research Projects of Higher Schools (Youth Projects) of Guizhou Provincial Department of Education (grant no. QJJ(2022)253), the financial support from the Science Research Foundation of Guizhou Education University (grant no. 2021BS026), the Opening Research Foundation of MOE Key Laboratory of Environmental Theoretical Chemistry for South China Normal University (grant no. 20210101), and the Japan Science and Technology Agency program "Support for Pioneering Research Initiated by the Next Generation" (JST SPRING, grant no. JPMJSP2136).

References

1 J. Zheng, S. Li, Y. Zhang, P. Zheng, X. Hu, Y. Fang, R. Duan, Q. Chen, *J. Mater. Chem. C* 2023,**11**, 7320-7330.
2 N. Fu, X. Liang, X. Wang, T. Gan, C. Ye, Z. Li, J. C. Liu, Y. Li, *J. Am. Chem. Soc.* 2023, **145**, 9540–9547.
3 F. Xu, B. Weng, *J. Mater. Chem. A*, 2023, **11**, 4473-4486.
4 Y. Yang, R. G. Agarwal, P. Hutchison, R. Rizo, A. V. Soudackov, X. Lu, E. Herrero, J. M. Feliu, *Nat. Chem.* 2023, **15**, 271–277.
5 S. N Upadhyay, S. Pakhira, *J. Mater. Chem. C*, 2021, **9**, 11331-11342.
6 S. Tian, Q. Tang, *J. Mater. Chem. C,* 2021, **9**, 6040-6050.
7 M. Ju, Z. Chen, H. Zhu, R. Cai, Z. Lin, Y. Chen, Y. Wang, J. Cao, X. Long, S. Yang, *J. Am. Chem. Soc.* 2023, **145**, 11215–11226.
8 Y. Ren, Y. Yang, M. Wei, *ACS Catal.* 2023, **13**, 8902–8924.
9 Y. Huang, F. Rehman, M. Tamtaji, X. Li, Y. Huang, T. Zhang, Z. Luo, *J. Mater. Chem. A*, 2022, **10**, 5813–5834.
10 B. M. Abraham, V. Parey, J. K. Singh, *J. Mater. Chem. C,* 2022, **10**, 4096-4123.
11 X. F. Gong, Y. L. Zhang, L. Zhao, Y. K. Dai, J. J. Cai, B. Liu, P. Guo, Q. Y. Zhou, I. Yagi, Z. B. Wang, *J. Mater. Chem. A*, 2022, **10**, 5971–5980.
12 X. Xie, L. Shang, X. Xiong, R. Shi, T. Zhang, T. *Adv. Energy Mater.* 2022, **12**, 21026388.
13 K. Shah, R. Dai, M. Mateen, Z. Hassan, Z. Zhuang, C. Liu, M. Israr, W. C. Cheong, B. Hu, R. Tu, et al. *Angew. Chem., Int. Ed.* 2022, **134**, e202114951.
14 P. Kumar, K. Kannimuthu, A. S. Zeraati, S. Roy, X. Wang, X. Wang, S. Samanta, K. A. Miller, M. Molina, *J. Am. Chem. Soc.* 2023, **145**, 8052–8063.
15 Y. Wu, H. Ma, Y. Feng, Z. Shi, Y. Yi, Y. Ding, J. Feng, W. Zhao, J. Sun, S. Dong, et al. *ACS Appl. Mater. Interfaces* 2022, **14**, 26803–26813.
16 M. Yang, R. Wu, S. Cao, Y. Li, S. Huo, W. Wang, Z. Hu, X. Xu, *Chem. Eng. J.* 2023, **451**, 138606.
17 J. Li, M. T. Sougrati, A. Zitolo, J. M. Ablett, I. C. Oğuz, T. Mineva, I. Matanovic, P. Atanassov, Y. Huang, I. Zenyuk, et al. *Nat. Catal.* 2021, **4**, 10−19.
18 Y. Shang, X. Duan, S. Wang, Q. Yue, B. Gao, X. Xu, *Chin. Chem. Lett.* 2022, **33**, 663–673.
19 M. Ma, Q. Tang, *J. Mater. Chem. C* 2022, **10**, 15948–15956.
20 H. Zhang, X. Jin, J. M. Lee, X. Wang, *ACS Nano* 2022, 16, 17572–17592.
21 K. Qu, Y. Zheng, Y. Jiao, X. Zhang, S. Dai, S. Z. Qiao, *Adv. Energy Mater.* 2017, **7**, 1602068.
22 C. Tang, Q. Zhang, *Adv. Mater.* 2017, **29**, 1604103.
23 Y. N. Gong, W. Zhong, Y. Li, Y. Qiu, L. Zheng, J. Jiang, H. L. Jiang, *J. Am. Chem. Soc.* 2020, **142**, 16723−16731.
24 G. Lu, K. Sun, Y. Lin, Q. Du, J. Zhang, K. Wang, P. Wang, *Nano Res.* 2022, **15**, 603–611.
25 F. A. Garces-Pineda, M. Blasco-Ahicart, D. Nieto-Castro, N. Lopez, J. R. Galan-Mascaros, *Nature Energy* 2019, **4**, 519−525.
26 C. Jia, X. Wang, H. Yin, W. Zhong, E. Sharman, Y. Luo, J. Jiang, *J. Mater. Chem. A*, 2021,**9**, 2093–2098.
27 Y. Zhou, R. Lu, X. Tao, Z. Qiu, G. Chen, J. Yang, Y. Zhao, X. Feng, K. Müllen, *J. Am. Chem. Soc.* 2023, **145**, 3647–3655.
28 W. Xue, Z. Zhu, S. Chen, B. You, C. Tang, *J. Am. Chem. Soc.* 2023, **145**, 4142–4149.
29 M. Gong, A. Mehmood, B. Ali, K. W. Nam, A. Kucernak, *ACS Catal.* 2023, **13**, 6661–6674.
30 J. Leverett, J. A. Yuwono, P. Kumar, T. Tran-Phu, J. Qu, J. Cairney, X. Wang, A. N. Simonov, R. K. Hocking, B. Johannessen, et al. *ACS Energy Lett.* 2022, **7**, 920–928.
31 X. Li, C. S. Cao, S. F. Hung, Y. R. Lu, W. Cai, A. I. Rykov, S. Miao, S. Xi, H. Yang, Z. Hu, et al. *Chem* 2020, **6**, 3440−3454.
32 P. Rao, J. Luo, D. Wu, J. Li, Q. Chen, P. Deng, Y. Shen, X. Tian, *Energy Environ. Mater.* 2023, **6**, e12371.
33 W. Liu, L. Zhang, X. Liu, X. Liu, X. Yang, S. Miao, W. Wang, A. Wang, T. Zhang, *J. Am. Chem. Soc.* 2017, **139**, 10790–10798.
34 W. Zhong, Y. Qiu, H. Shen, X. Wang, J. Yuan, C. Jia, S. Bi, J. Jiang, *J. Am. Chem. Soc.* 2021, **143**, 4405–4413.
35 Q. Yang, Y. Jiang, H. Zhuo, E. M. Mitchell, Q. Yu, *Nano Energy* 2023, **111**, 108404.
36 W. Yuan, Y. Ma, H. Wu, L. Cheng, *J. Energy Chem.* 2022, **65**, 254–279.
37 A. Kumar, V. K. Vashistha, D. K. Das, S. Ibraheem, G. Yasin, R. Iqbal, T. A. Nguyen, R. K. Gupta, M. R. Islam, *Fuel* 2021, **304**, 121420.
38 M. Li, H. Wang, W. Luo, P. C. Sherrell, J. Chen, J. Yang, *Adv. Mater.* 2020, **32**, 2001848.
39 C. Zhang, H. Wang, H. Yu, K. Yi, W. Zhang, X. Yuan, J. Huang, Y. Deng, G. Zeng, *Adv. Energy Mater.* 2022, **12**, 2200875.
40 C. J. Cramer, D. G. Truhlar, *Phys. Chem. Chem. Phys.* 2009, **46**, 10757−10816.
41 M. Frisch, et al. Gaussian 16, revision C.01; Gaussian, Inc.: Wallingford, CT, 2016.
42 Y. Li, P. Su, J. Jiang, Z. Ke, *ACS Catal.* 2021, **11**, 13452−13462.

43 J. Liu, Y. Li, J. Jiang, Yan Liu, Z. Ke, *ACS Catal.* 2021, **11**, 6186−6192.
44 J. Lin, Y. Lin, Z. Ke, *J. Phys. Chem. A* 2023, **127**, 4375−4387.
45 Y. Li, H. Liang, Y. Liu, J. Lin, Z. Ke, *ACS Catal.* 2023, **13**, 13008−13020.
46 F. Weigend, R. Ahlrichs, *Phys. Chem. Chem. Phys.* 2005, **7**, 3297–3305.
47 D. Andrae, U. Haeussermann, M. Dolg, H. Stoll, H. Preuss, *Theor. Chim. Acta.* 1990, **2**, 123–141.
48 S. Grimme, J. Antony, S. Ehrlich, H. A. Krieg, *J. Chem. Phys.* 2010, **15**, 154104.
49 K. Fukui, *J. Phys. Chem.* 1970, **23**, 4161–4163.
50 K. Fukui, *Acc. Chem. Res.* 1981, **12**, 363–368.
51 T. Lu, F. Chen, F. *J. Comput. Chem.* 2012, **33**, 580–592.
52 C. Choi, S. Back, N. Y. Kim, J. Lim, Y. H. Kim, Y. Jung, *ACS Catal.* 2018, **8**, 7517–7525.
53 D. A. Bulushev, M. Zacharska, A. S. Lisitsyn, O. Y. Podyacheva, F. S. Hage, Q. M. Ramasse, U. Bangert, L. G. Bulusheva, *ACS Catal.* 2016, **6**, 3442−3451.
54 G. Luo, Y. Jing, Y. Li, *J. Mater. Chem. A* 2020, **8**, 15809-15815.
55 Y. Ying, X. Luo, J. Qiao, H. Huang, *Adv. Funct. Mater.* 2020, **31**, 2007423
56 Z. Zhang, J. Xiao, X. J. Chen, S. Yu, L. Yu, R. Si, Y. Wang, S. Wang, X. Meng, Y. Wang, et al. *Angew. Chem., Int. Ed.* 2018, **57**, 16339-16342.
57 Y. Wang, B. J. Park, V. K. Paidi, R. Huang, Y. Lee, K. J. Noh, K. S. Lee, J. W. Han, *ACS Energy Lett.* 2022, **7**, 640–649.
58 C. Jia, Q. Wang, J. Yang, K. Ye, X. Y. Li, W. Zhong, H. Shen, E. Sharman, Y. Luo, J. Jiang, *ACS Catal.* 2022, **12**, 3420–3429.
59 C. Jia, Y. Zhang, X. Wang, W. Zhong, O. V. Prezhdo, Y. Luo, J. Jiang. *J. Mater. Chem. A* 2020, **8**,12485-12494.
60 J. Pan, X. Li, Y. Zhu, J. Zhou, Z. Zhu, C. Li, X. Liu, X. Liang, Z. Yang, Q. Chen, et al. *J. Am. Chem. Soc.* 2023, **145**, 18748–18752.
61 B. Kumar, M. Asadi, D. Pisasale, S. Sinha-Ray, B. A. Rosen, R. Haasch, J. Abiade, A. L. Yarin, A. Salehi-Khojin, *Nat. Commun.* 2013, **4**, 2819.
62 S. Sinhababu, M. R. Radzhabov, J. Telser, N. P. Mankad, *J. Am. Chem. Soc.* 2022, **144**, 3210–3221.
63 Q. Wang, B. Jin, M. Hu, C. Jia, X. Li, E. Sharman, J. Jiang, *J. Phys. Chem. C* 2021, **125**, 5616-5622.
64 J. Yang, L. Lv, S. Cui, C. Sun, L. Sun, B. Shi, E. Sharman, J. Jiang, C. Jia, *J. Phys. Chem. Lett.* 2022, **13**, 8851–8857.
65 C. Hu, L. Zhang, J. Gong, *Energy Environ. Sci.* 2019, **12**, 2620–2645.